Measurements of the Ground-State Polarizabilities of Cs, Rb, and K using Atom Interferometry

Maxwell D. Gregoire,[1] Ivan Hromada,[1] William F. Holmgren,[1] Raisa Trubko,[2] and Alexander D. Cronin[1,2]

[1] *Department of Physics, University of Arizona, Tucson, AZ 85721*
[2] *College of Optical Sciences, University of Arizona, Tucson, AZ 85721*

(Dated: June 22, 2015)

We report absolute and ratio measurements of ground-state, static, electric-dipole polarizabilities of Cs, Rb, and K atoms using a Mach-Zehnder atom interferometer with an electric field gradient. Our measurements provide benchmark tests for atomic structure calculations, and our measurement of α_{Cs} helps with interpretation of parity non-conservation data. We measured polarizabilities of $\alpha_{\mathrm{Cs}} = 59.51(3)(11)$, $\alpha_{\mathrm{Rb}} = 47.50(3)(9)$, and $\alpha_{\mathrm{K}} = 43.15(2)(8)$ (in the form: measurement(stat. error)(total error)) and ratios of $\alpha_{\mathrm{Cs}} : \alpha_{\mathrm{Rb}} = 1.2528(11)$, $\alpha_{\mathrm{Cs}} : \alpha_{\mathrm{K}} = 1.3791(9)$, and $\alpha_{\mathrm{Rb}} : \alpha_{\mathrm{K}} = 1.1008(10)$. We are the first to measure Cs polarizability with atom interferometry because we were able to measure the beam velocity distribution using phase choppers rather than by obtaining resolved diffraction, which is difficult to obtain with Cs. We also increased the precision of our measurements with more advanced modeling of the beam profile and new understanding of systematic errors.

Sample citation[1].

INTRODUCTION

We present absolute and ratio measurements of the static electric-dipole polarizabilities of Cs, Rb, and K made using a Mach-Zehnder three-grating atom interferometer in an electric field gradient [Bermann][Cronin RMP]. This is the first time atom beam interferometry has ever been used to measure Cs polarizability. Measuring polarizability requires measuring the velocity of the atom beam, but previously, we could not obtain resolved diffraction with a Cs beam and therefore could not measure its velocity using diffraction as we did in our earlier work [HRL10]. We overcame this obstacle by measuring the beam velocity using phase choppers, a successor to mechanical choppers invented by someone [cite it] that we are first to implement [choppers paper] and use here for measurement of fundamental atomic properties. Phase choppers are a pair of electric field gradients chopped on and off at varying frequencies that are tuned to apply $+\pi$ and $-\pi$ phase shifts, respectively; the percentage of atoms which receive a net $\pm\pi$ phase shift depends on the chopping frequency and atom velocity distribution and is observed by measuring loss of contrast.

High-precision static-polarizability measurements are used to test atomic structure calculation methods used to calculate polarizabilities, van der Waals coefficients, state lifetimes, branching ratios, and indices of refraction [...and all that]. The quantum many-body theories with relativistic corrections required to describe atoms with many electrons must be highly sophisticated in order to calculate the atomic transition dipole matrix elements accurately in a reasonable amount of computing time [MSC10]. There are many competing atomic structure calculation methods that produce different results.

Testing Cs atomic structure calculations by measuring α_{Cs} is particularly important for parity non-conservation (PNC) research. The coupling strength of Z^0-mediated interactions between the Cs chiral valence electron and nuclear neutrons is proportional to ρ, the electron density near the nucleus, and the nuclear weak charge Q_W. To calculate Q_W from measurements of coupling strength, PNC researchers must use atomic structure calculations to determine ρ [Bouchiat x2, 97][Dzuba Flam 12].

We can also cross-check our results against polarizabilities calculated using recent high-precision measurements of state liftimes. These lifetime-based values have uncertainty comparable to that of our own.

We were also able to make these ratio measurements with record precision through a deeper understanding of the atom beam as having finite thickness and divergence and interacting with a finitely-sized detector, especially in the context of the phase choppers [lens paper]. We eliminated systematic errors by polarizing the atoms with two parallel, oppositely-charged cylinders rather than one charged cylinder and a grounded plane [HRL10]–the new geometry allows us to more precisely determine the beam's position in the electric field and eliminates systematic error due to the rotation of the Earth.

Measuring alkali static polarizabilities as a means of testing atomic structure calculations has been of interest to the physics community since 1934 [H. Scheffers and J. Stark, Phys. Z. 35, 625 (1934)], and has been accomplished using deflection [ScSt34, ChZo62, HaZo74], the E-H gradient balance technique [SPB611, MSM74], time-of-flight measurements of atoms in a fountain [AmGo03], and, most recently, atom interferometry [ESC95, MJB06, HRL10]. It is likely that atom interferometry will continue to be the tool of choice for precision polarizability measurements.

APPARATUS DESCRIPTION AND ERROR ANALYSIS

The three-grating Mach-Zehnder atom interferometer we use to make our measurements is shown in Fig. 1. We pass a thermal, supersonic atom beam [Scoles] through three silicon nitride gratings of period $d_g = 100$ nm. The detector is a platinum Langmuir-Taylor detector [DML02].

Our method of measuring the velocity distribution and our method of measuring polarizability involve applying a phase shift using non-uniform electric fields created by either a cylinder at voltage V next to a grounded plane or two parallel cylinders at $\pm V$ forming an effective ground plane. The effective line charge density

$$\lambda = 2\pi\epsilon_0 V \ln^{-1}\left(\frac{a+R+b}{a+R-b}\right) \tag{1}$$

exists a distance $b = a\sqrt{1+2R/a}$ away from the ground plane, where a is the distance between the ground plane and the closest cylinder edge, R is the cylinders' radius, and $\hat{x}$ and $\hat{z}$ are shown in Fig. 1.

When an atom with polarizability α enters an electric field, it's energy shifts by $U_{Stark} = \frac{1}{2}\alpha\left|\vec{E}\right|^2$. We can use the WKB approximation (since $U_{Stark} \ll U_{kinetic}$) and the Residue Theorem to compute the total phase acquired by an atom traveling along the beamline a distance x_b away from the ground plane. The diffraction angles θ_d in our interferometer are on the order of 10^{-6} rad, so we can approximate that atoms always travel parallel to the beamline. That accumulated phase is

$$\phi(v,x) = \frac{\lambda^2\alpha}{\pi\epsilon_0^2\hbar v}\left(\frac{b}{b^2-x_b^2}\right) \tag{2}$$

where v is the atom's velocity.

Therefore, the phase shifts for the interferometers on the $j=+1$ and $j=-1$ sides of the beamline (see Fig. 1) are

$$\begin{aligned}\Phi_{\vec{E},1}(v,x_b) &= \phi(x_b+\theta_d z_0) - \phi(x_b)\\ \Phi_{\vec{E},-1}(v,x_b) &= \phi(x_b) - \phi(x_b-\theta_d z_0)\end{aligned} \tag{3}$$

where z_0 is the longitudinal distance between the $z=0$ point in the field and whichever of the 1st or 3rd gratings is closest.

Velocity Measurement

We model the atom beam's velocity distribution as a Gaussian distribution

$$P(v)dv = \frac{r}{v_0\sqrt{2\pi}} e^{-\frac{r^2(v-v_0)^2}{2v_0^2}} \tag{4}$$

where v_0 is the mean velocity and $r = v_0/\sigma_v$ is a measure of the distribution's sharpness. To measure v_0 and r, we use phase choppers. Each phase chopper is a charged wire near a physical ground plane. Chopper 1 is between the first two gratings and chopper 2 is a distance z_{c1c2} downstream of chopper 1, between the last two gratings (see Fig. 1). The voltage on the wire and the distance between the beam and the ground plane are chosen such that chopper 1 applies a $+\pi$ phase shift and chopper 2 applies a $-\pi$ phase shift. When we pulse the choppers on and off at frequency f_c, an atom may receive a net phase shift of $\pm\pi$ or 0 depending on its velocity. Therefore, v_0, r, and f_c determine the fraction of total atoms in the beam which receive a $\pm\pi$ phase shift. This fraction can be quantified by measuring contrast loss C/C_{ref}. To measure v_0 and r, we measure C/C_{ref} vs f_c.

We have identified a number of v_0-dependent systematic errors associated with phase chopper velocity distribution measurements. These errors must be eliminated in order to make polarizability ratio measurements of atomic species, which may typically run at different v_0.

In our previous work [lens paper], we documented the systematic errors that would appear if we were to not accurately know $\Delta L = L_1 - L_2$, where L_1 is the distance between gratings 1 and 2 and L_2 is the distance between gratings 2 and 3. There are two components to this error contribution. The first is that changing ΔL shifts the interference fringes away from the beamline. We call this phase shift the separation phase:

$$\Phi_{sep,j} = \frac{2\pi}{d_g}\left(\theta_{inc} + \frac{j}{2}\theta_d\right)\Delta L \tag{5}$$

where θ_{inc} is the incident angle of a given atom with de-Broglie wavelength λ_{dB} on grating 1. The second component of the error contribution has to do with the longitudinal localization of the interference pattern that exists a distance L_1 downstream of grating 2. The contrast of that pattern decreases as the observer moves longitudinally in either direction [thry paper on this]. Furthermore, the electric fields, such as those created by the phase choppers, act as lenses that move the contrast maximum [lens paper]. Thus the choppers change the contrast simply by turning on, and changing the longitudinal location of the 3rd grating changes how the choppers modify the contrast.

We significantly reduced systematic error by modeling how the collimating slits define the beam's width and divergence and by considering the finite width of the detector, both of which determine how likely it is for atoms of a given velocity to be detected and thus contribute to a measurement of v_0. This new model also added elements to the error budget: the lateral offset of the detector from the beamline $\Delta x_{detector}$ and the gratings' diffraction efficiencies determine how likely it is for atoms with certain velocities to be detected.

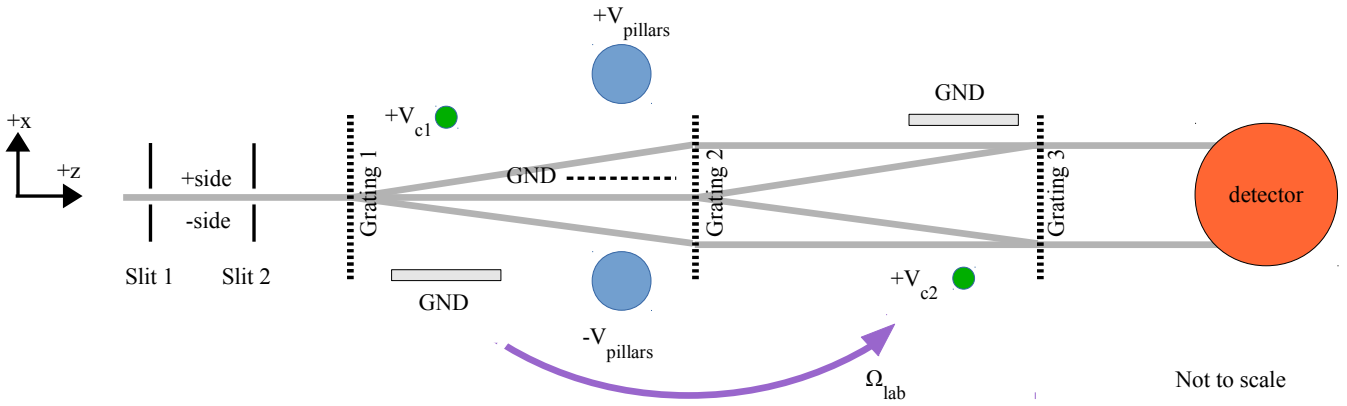

FIG. 1. (Color online) Diagram of the atom interferometry apparatus. The supersonic atom beam is collimated by two slits before entering the gratings.

We find that as $|\Delta L|$ increases, the measured v_0 and r become more and more dependent on the beam width, beam divergence, and detector width. Accordingly, we set $\Delta L = 0$ to reduce contributions to $\Delta v_0/v_0$ from other sources of uncertainty. We begin each day of measurements by setting ΔL to 0, eliminating the need to consider Φ_{sep}. We know that if Φ_{sep} were nonzero, we would see the measured phase change as a function of $\Delta x_{detector}$, the detector's lateral position in the beamline. We set $\Delta L = 0$ by finding the ΔL for which the measured phase no longer changes as a function of $\Delta x_{detector}$.

If the interferometer grating bars are significantly non-vertical, it can become necessary to consider the phase shift induced by the component of gravitational acceleration in the plane of the interferometer, which is given by

$$\Phi_{accel} = \frac{\pi g \sin\theta_g (L_1 + L_2)^2}{2 d_g v^2} \tag{6}$$

where θ_g is the tilt of the grating bars with respect to vertical. However, we eliminated the need to consider Φ_{accel} by rotating our grating bars so that they were sufficiently vertical. We measured θ_g to be $0 \pm 2mrad$. Only if $|\theta_g| >$???? would we need to add Φ_{accel} to our analysis.

Taking all these effects into account, our more complete model for contrast loss as a function of chopping frequency is

$$\begin{aligned}\frac{C}{C_{ref}}(f_c) = \frac{1}{2}\sum_{j=-1,1} f_c \int_0^{1/f_c}\int_{w_1/2}^{w_1/2}\int_{w_2/2}^{w_2/2}\int_0^{\infty} \\ P(v) D_j(x_1,x_2,v) C_{env}(t) \\ \times e^{i(\Phi_{c1,j}(v,x_1,x_2,t)+\Phi_{c2,j}(v,x_1,x_2,t-l/v))} \\ \times e^{i(\Phi_{sep,j}(v,x_1,x_2)+\Phi_{accel}(v)+\Phi_{sag}(v))} dv dx_2 dx_1 dt\end{aligned} \tag{7}$$

To account for beam width and divergence, we integrate over positions x_1 and x_2 in the two collimating slits, which have widths w_1 and w_2. $D_j(x_1, x_2, v)$ is the probability that a given atom will hit the detector, and $C_{env}(t)$ represents the longitudinal motion of the interference pattern as the choppers turn on and off (see [lens paper] for how we determined $C_{env}(t)$ experimentally). $\Phi_{sag}(v)$ is the Sagnac phase, or the phase shift induced by the Earth's rotation[ref for that], and is given by

$$\Phi_{sag}(v) = \frac{4\pi L_2^2 \Omega_{lab}}{d_g v} \tag{8}$$

The rotation rate of the interferometer, Ω_{lab}, is the product of the Earth's rotation rate and the sine of the lab's lattitude. During times t when the choppers are on, the chopper-induced phases $\Phi_{ci,j}(v, x_1, x_2)$ are adapted from

TABLE I. Systematic error budget for measurements of v_0 and r. Some error sources are expressed as fractional uncertainties, some as absolute uncertainties.

Error Source x	$\Delta x/x$	$\Delta v_0/v_0 \times 1000$	$\Delta r/r \times 1000$
w_1	260	0.05	1.0
w_2	260	0.09	6.6
$w_{detector}$	100	0.05	4.2
a_{c1}	25	0.005	0.1
a_{c2}	28	0.03	2.9
$z_{c1,c2}$	.20	0.20	0.1
Ω_{lab}	62	0.003	1.2
$C_{env}(t)$ width	100	0.06	2.7
Error Source x	Δx	$\Delta v_0/v_0 \times 1000$	$\Delta r/r \times 1000$
$\Delta x_{detector}$	20 μm	0.006	0.15
ΔL	50 μm	0.098	6.0
Total Sys. (ppt)		0.28	11

Eqn. 3 and given by

$$\Phi_{c1,j}(v,x_1,x_2) = \frac{A_{c1}}{v} j \times \left(\frac{1}{b_{c1}^2 - (x_{c1} + \frac{(x_2-x_1)}{z_{s1,s2}} z_{s1,c1} + x_2 + j\theta_d z_{g1,c1})^2} - \frac{1}{b_{c1}^2 - (x_{c1} + \frac{(x_2-x_1)}{z_{s1,s2}} z_{s1,c1} + x_2)^2} \right)$$

$$\Phi_{c2,j}(v,x_1,x_2) = \frac{A_{c1}}{v} j \times \left(\frac{1}{b_{c2}^2 - (x_{c2} - \frac{(x_2-x_1)}{z_{s1,s2}} z_{s1,c2} - x_2 - j\theta_d z_{g1,g2})^2} - \frac{1}{b_{c2}^2 - (x_{c2} - \frac{(x_2-x_1)}{z_{s1,s2}} z_{s1,c2} - x_2 - j\theta_d z_{g2,c2})^2} \right) \quad (9)$$

In the above equations, subscripts sn and gn on longitudinal distances z represent collimating slit n and grating n, respectively. A_{c1} and A_{c2} are undetermined constants that represent $\lambda_{ci}^2 \alpha / \pi \epsilon_0^2 \hbar$ from Eqn. 2.

Instead of requiring accurate knowledge of the chopper voltages and geometries, we measure A_{ci} indirectly. We turn chopper i on and off with a 50 second period to observe the applied phase shift $\Delta\Phi = \Phi_{c1,on} - \Phi_{ref}$ and then solve for A_{ci}. When chopper i is off, we observe the reference phase and contrast

$$C_{ref} e^{\Phi_{ref}} = C_0 e^{\Phi_0} \frac{1}{2} \sum_{j=-1,1} \int_0^\infty \int_{w_1/2}^{w_1/2} \int_{w_2/2}^{w_2/2} P(v) e^{\Phi_{sag}(v) + \Phi_{accel}(v) + \Phi_{sep,j}(v)} dv \quad (10)$$

where C_0 is the contrast that would be observed in the absence of $\Phi_{sag}(v)$, $\Phi_{accel}(v)$, and $\Phi_{sep}(v)$, and Φ_0 is an arbitrary phase constant. When chopper i is on, we instead observe

$$C_{ci,on} e^{\Phi_{ci,on}} = C_0 e^{\Phi_0} \frac{1}{2} \sum_{j=-1,1} \int_0^\infty \int_{w_1/2}^{w_1/2} \int_{w_2/2}^{w_2/2} P(v) e^{\Phi_{ci,j}(v,x_1,x_2) + \Phi_{sag}(v) + \Phi_{accel}(v) + \Phi_{sep,j}(v)} dv \quad (11)$$

Fig. 2 shows an example of a C/C_{ref} vs f_c measurement. For tutorial purposes, Eqns. (7), (10), and (11) include Φ_{sep} and Φ_{accel} even though we have tuned our apparatus so that we need not include them in our analysis.

The error budget for velocity distribution measurement is given in Table I. The measured values of v_0 and r also have statistical error in addition to uncertainty in the fit of measured $C/C_{ref}(f_c)$ to the model. Uncertainty in the measurement of $\Delta\Phi = \Phi_{c1,on} - \Phi_{ref}$ leads to uncertainty in A_{ci}, which in turn propagates forward as additional uncertainty in v_0 and r.

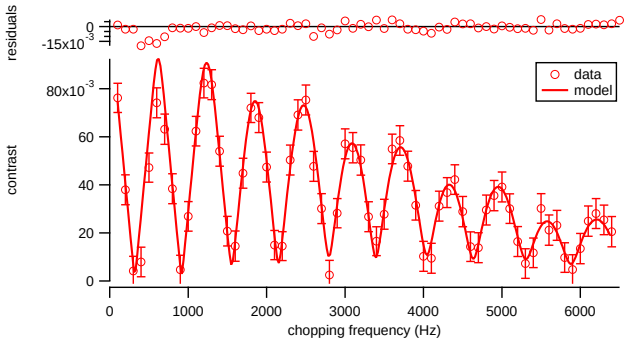

FIG. 2. (Color online) An example of a measurement of contrast loss vs. phase chopper frequency for a Cs beam.

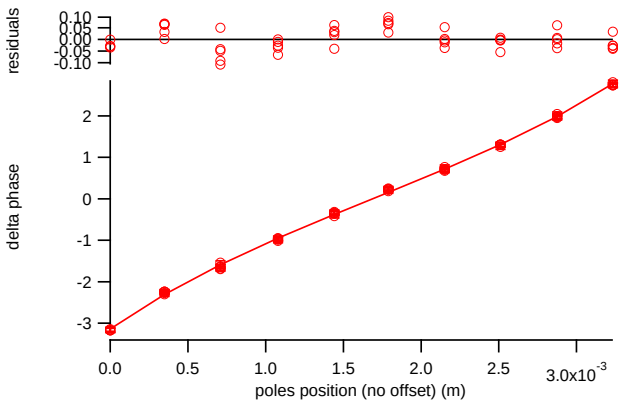

FIG. 3. (Color online) An example of a measurement of phase shift vs lateral position of the pillars for a Rb beam.

Polarizability Measurement

We measure the atoms' polarizability by scanning the gap between two parallel, oppositely charged, 1/2-inch pillars across the beam, turning the field on and off as it scans, to observe the phase shift $\Delta\Phi = \Phi_{pillars,on} - \Phi_{ref}$ applied by the pillars as a function x_b (see an example in Fig. 3). Phi_{ref} is once again the reference phase and contrast observed when there are no polarizing electric fields present. When the pillars are on, we instead observe

$$C_{\vec{E}\ on} e^{\Phi_{\vec{E}\ on}} = C_0 e^{\Phi_0} \frac{1}{2} \sum_{j=-1,1} \int_0^\infty P(v) \times e^{\Phi_{\vec{E},j}(v,x_b) + \Phi_{sag}(v) + \Phi_{accel}(v) + \Phi_{sep,j}(v)} dv \quad (12)$$

We determine x_b by finding the pillars position for which the phase shift is null. This eliminates the error in our previous measurements associated with measuring the distance between the beam and the physical ground plane

TABLE II. Error budget for polarizability measurements. The uncertainties in knowledge of v_0 and r are propagated forward from Table I. Some error sources are expressed as fractional uncertainties, some as absolute uncertainties.

Error Source x	$\Delta x/x$ (ppt)	$\Delta\alpha/\alpha$ (ppt)
d_g	0.1%	1
$V_{pillars}$	.5	1
$a_{pillars}$	0.25	0.7
$R_{pillars}$	0.16	0.07
v_0	0.28	0.56
r	11	0.28
$z_{g1,pillars}$	0.3	0.6
Error Source x	Δx	$\Delta\alpha/\alpha$ (ppt)
dimer fraction	0.02	0.46
ΔL	50 μm	0.16
Total Sys. (ppt)		1.9

[HRL10]. Because $\Phi_{\vec{E}}$ depends on α, we can measure α by fitting our model of $\Delta\Phi(x)$ to the data.

The error budget for the absolute polarizability measurements is given in Table II. The only new terms are uncertainty in ΔL because of separation phase (Eqn. 5), and uncertainty in grating tilt because of acceleration phase (Eqn. 6).

We constructed the new pillars using steel rods, the widths of which were accurately known to 1μm. This reduced the contribution to $\Delta\alpha/\alpha$ from uncertainty in pillars radius by about a factor of 10. The new pillars have a virtual ground plane between then rather than consisting of one pillar and a physical ground plane as they did in our previous work; we found that being able to measure the phase shift with the beam on both sides of the ground plane eliminated the need to consider Φ_{sag}.

We reduced some error contributions simply by measuring things more carefully. We reduced $\Delta\alpha/\alpha$ due to uncertainty in the pillars' voltage by a factor of 3 by independently calibrating our voltage supplies. We also reduced $\Delta\alpha/\alpha$ due to uncertainty in distance between the pillars and the effective ground plane by sweeping the pillars across the atom beam and observing how far the pillars traveled between points at which the atom beam half-eclipsed each pillar. We were able to measure the distance between the first grating and the pillars to 1/4 mm accuracy rather than 2 mm accuracy.

It is important to note that we also don't need to consider Φ_{accel} in our polarizability analysis as well as in our velocity distribution analysis because the grating bars are sufficiently vertical. Therefore, Φ_{sag}, Φ_{accel}, and Φ_{sep} are included in Eqn. 12 for tutorial purposes only–our result is unaffected if we remove them.

Additionally, we found that modeling the beam's thickness and divergence was unnecessary for analysis of polarizability data unless $|\Delta L|$ exceeds about 100 μm. Because we keep ΔL close to 0, we only need to integrate over velocity in our analysis.

TABLE III. Absolute measurements of Cs, Rb, and K static, ground-state polarizabilities.

Atom	avg v_0 (m/s)	avg r	α(stat.)(sys.) ($\AA^2$)	χ^2/DoF
Cs	1587	21	59.51(3)(11)	1.02
Rb	1891	24	47.50(3)(9)	1.05
K	2118	14	43.15(2)(8)	1.26

Data Analysis

We measure the velocity distribution between every 4 scans of the pillars across the beam. We interpolate the velocity distribution between measurements to estimate it for each pillars scan. The error bars on each interpolated v_0 and r value are due to the error bars on neighboring measurements and the different ways we believe v_0 and r might be reasonably interpolated. For example, we believe linear and cubic spline interpolations are reasonable, so the error bars at a given time take into account the differences between those interpolations–a larger difference between reasonable interpolations leads to larger error bars on interpolated values. That error is then propagated forward and combined with the statistical error of the fit to $\Delta\Phi$ vs x_b to determine the error bars on the polarizability measurements. Fig. 4 shows an example of interpolations between v_0 measurements at the times of various pillars scans.

RESULTS

Table III shows our absolute measurements of Cs, Rb, and K polarizability and their statistical and systematic errors. The error reported is the standard error of the mean. Table III also shows χ^2/(degree of freedom) for each measurement; we can see that we are operating near the shot-noise limit.

Table IV shows our ratio measurement results. Because we used the same apparatus for each absolute measurement, we can say that the systematic errors mentioned previously do not contribute to the ratio measurement errors. This is important because even if a systematic error causes our absolute measurements to be incorrect, our ratios should still be reliable. *This statement does not jibe with the earlier statement that some systematic errors are velocity-dependent. I'm looking into this now*

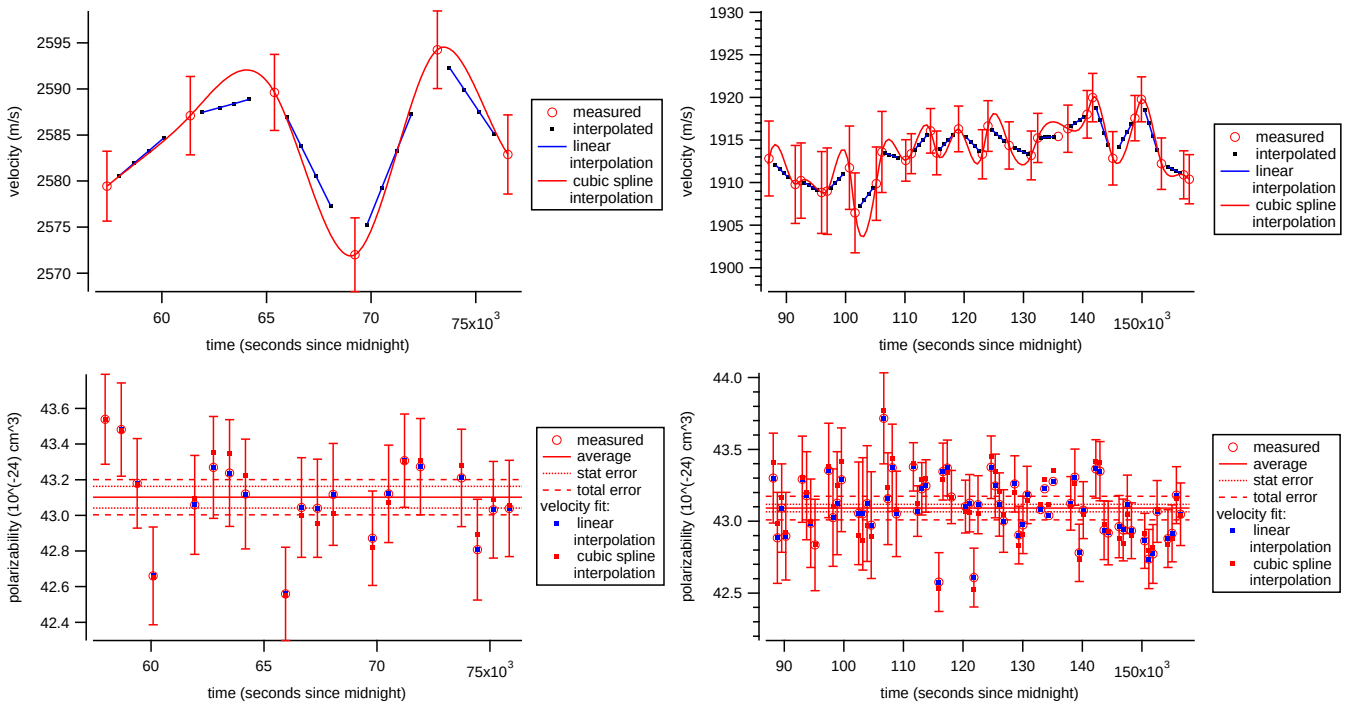

FIG. 4. (Color online) The results of v_0 (top) and α_K (bottom) measurements taken during two different days (left and right). Both linear and cubic spline interpolations between v_0 measurements are reasonable, and higher differences between the two interpolations during α_K measurements increase the error bars on said measurements. For these data, we chose to use linear interpolation because we believe it more accurately represents v_0 vs t–the cubic spline interpolation sometimes gains too much curviture, especially when back-to-back velocity measurements, such as those in the top-left, yield results that differ by an error bar. The red dots on the bottom graphs show what the measured α_K would be if we were to use cubic spline interpolation instead. The top graphs show some typical structures that occur in v_0 vs time. This figure also demonstrates how we obtain the same α_K for very different velocities.

TABLE IV. Ratio measurements of Cs, Rb, and K static, ground-state polarizabilities.

Atoms	ratio(stat.)
Cs:Rb	1.2528(11)
Cs:K	1.3791(9)
Rb:K	1.1008(10)

COMPARISONS WITH OTHER WORK

Fig. 5 compares our polarizability measurements with theoretical calculations, semi-empirical calculations, and experimental measurements subsequent to and including Molof *et al.*'s and Hall *et al.*'s 1974 measurements [Mol74][Hal74]. Our absolute measurements are consistent with all previous absolute measurements, though our Cs measurement is only barely consistent with Amini and Gould's and our Rb measurement is only barely consistent with our lab's previous measurement. At present, we don't have an explanation for these almost-discrepancies. We acknowledge the possibility of a systematic error in our experiment we are as of yet unaware of, and we hope to calibrate our measurements in the future by measuring a well-known polarizability, such as that of lithium or metastable helium.

Fig. 5 also compares our ratios to other theoretical, semi-empirical, and experimental ratios. Our ratios are also consistent with all previous measurements, though our Rb:K ratio is barely consistent with our lab's previous Rb:K ratio.

Additionally, we can compare our measurements to polarizabilities calculated using recent high-precision measurements of state lifetimes. For an atom in state i, the polarizability can be written in terms of Einstein A coefficients as

$$\alpha_i = \frac{3c^3}{2} \sum_{k \neq i} \frac{A_{ki}}{\omega_{ik}^4} \frac{g_k}{3g_i} + \alpha_{core} + \alpha_{tail} \qquad (13)$$

where ω_{ik} is the transition frequency between states i and k and $g_n = 2J_n + 1$ is the degeneracy factor for state n. In our case, state i is the ground state. α_{core} is the polarizability of the core electrons, and α_{tail} approximates all the terms not explicitly included in the sum; we will only be using measured lifetimes for $NS - NP$

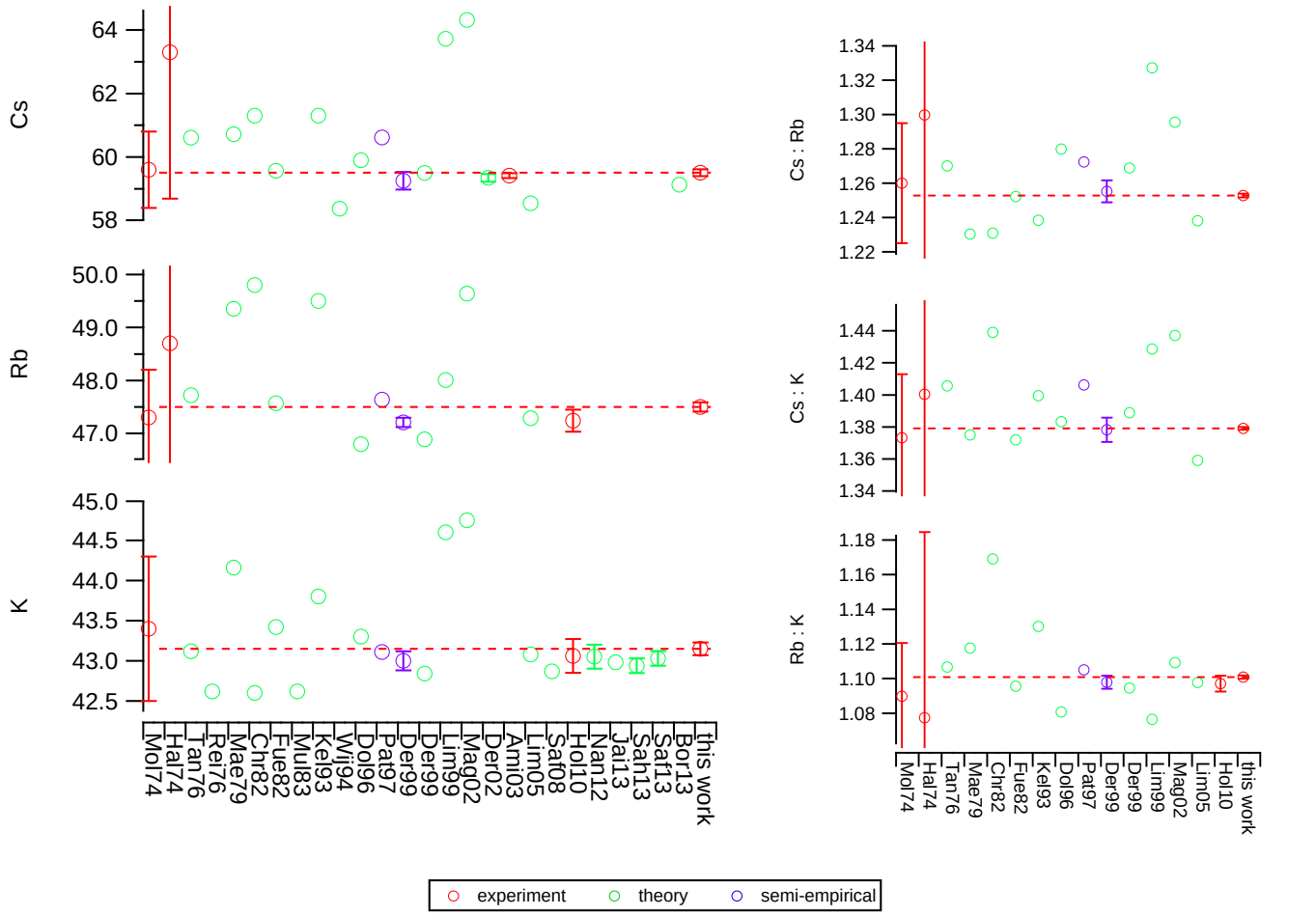

FIG. 5. (Color online) Our absolute measurements (left) and ratio measurements (right) compared with other measurements, *ab initio* calculations, and semi-empirical calculations. The references are represented on the x-axis by the first three letters of the first author's last name followed by the year of publication. Reference Der99 used experimentally-determined electric dipole matrix elements, while reference Pat97 used experimentally-determined energy levels [Der99][Pat97]. *TODO: proper y axis labels–can you type α_{Cs} in IGOR, or do I have to paste it in?*

transitions. We use Lim *et al.*'s calculated core polarizabilities of $\alpha_{core,\mathrm{K}} = 0.818(6)\mathring{A}^3$, $\alpha_{core,\mathrm{Rb}} = 1.350(6)\mathring{A}^3$, and $\alpha_{core,\mathrm{Cs}} = 2.341(15)\mathring{A}^3$ [Lim02]. Furthermore, Derevianko and Porsev calculated that $\alpha_{tail,\mathrm{Cs}} = 0.162\mathring{A}^3$ [Der02]. Because we lack values for $\alpha_{tail,\mathrm{Rb}}$ and $\alpha_{tail,\mathrm{K}}$ and because $\alpha_{tail,\mathrm{Cs}}$ only accounts for 0.27% of α_{Cs}, we can approximate for these purposes that α_{tail} accounts for 0.27% of α for Rb and K as well. The ω_{0k} values are calculated using transition wavelengths reported by NIST [ref for this].

Fig. 6 compares our measurements with these lifetime-based results. Our measurements are significantly higher than most of the values based on recent lifetime measurements. Because the lifetime measurements were all made by different people using different experimental methods, these discrepancies strongly suggest that our absolute polarizability measurements are too high and require calibration.

OUTLOOK

We are currently exploring ways to measure the polarizability of metastable He, the polarizability of which can be easily calculated. By measuring $\alpha_{\mathrm{Cs}} : \alpha_{He*}$, we could report an absolute measurement of α_{Cs} with uncertainty comparable to that of the ratios reported here for the benefit of PNC research and as a calibration of the measurements presented in this work.

We are also exploring electron-impact ionization schemes for atom detection, which would allow us to detect a much broader range of atoms and molecules. Our

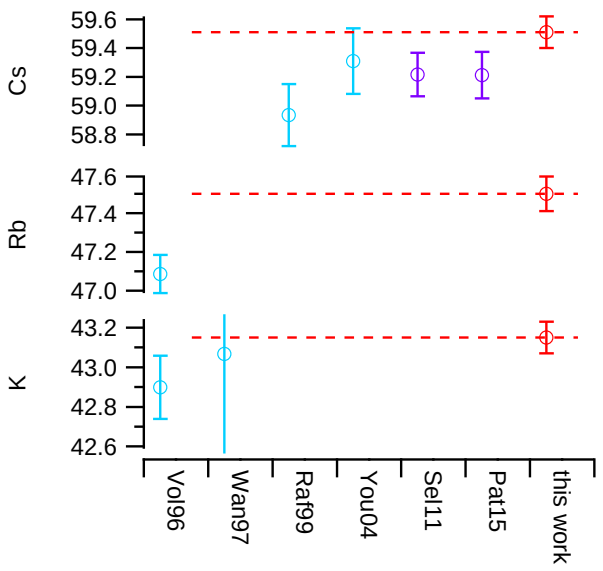

FIG. 6. (Color online) Our measurements (red) are compared with polarizabilities calculated using experimentally measured lifetimes. Light blue points were calculated using both $Ns - NP_{1/2}$ and $Ns - NP_{3/2}$ lifetimes, while dark purple points were calculated using $Ns-NP_{3/2}$ lifetimes and the $Ns-NP_{3/2}$:$Ns-NP_{1/2}$ ratio provided by Young *et al.*[You94]

Langmuir-Taylor [DML02] only allows us to detect alkali metals and some alkaline-Earth metals. Installing a new, "universal" detector would allow us to broaden the scope of atom interferometry as a precision measurement tool.

This work is supported by NSF Grant No. 1306308 and a NIST PMG. M.D.G. and R.T. are grateful for NSF GRFP Grant No. DGE-1143953 for support.

[1] I. Hromada, R. Trubko, W. F. Holmgren, M. D. Gregoire, and A. D. Cronin, Phys. Rev. A **89**, 033612 (2014).